

Wind pressure and buckling of grouped steel tanks

Genock Portela[†]

General Engineering Department, University of Puerto Rico, Mayagüez, Puerto Rico 00681-9044, USA

Luis A. Godoy[‡]

*Civil Infrastructure Research Center, Department of Civil Engineering and Surveying,
University of Puerto Rico, Mayagüez, Puerto Rico 00681-9041, USA*

(Received December 29, 2005, Accepted November 22, 2006)

Abstract. Wind tunnel experiments on small scale groups of tanks are reported in the paper, with the aim of evaluating the pressure patterns due to group effects. A real tank configuration is studied in detail because one tank buckled during a hurricane category 3. Three configurations are studied in a wind tunnel, two with several tanks and different wind directions, and a third one with just one blocking tank. The pressures were measured in the cylindrical part and in the roof of the tank, in order to obtain pressure coefficients. Next, computational buckling analyses were carried out for the three configurations to evaluate the buckling pressure of the target structure. Finally, imperfection-sensitivity was investigated for one of the configurations, and moderate sensitivity was found, with reductions in the maximum load of the order of 25%. The results help to explain the buckling of the tank for the levels of wind experienced during the hurricane.

Keywords: buckling; shells; tanks; wind tunnel; wind pressures.

1. Introduction

The recent wave of hurricanes impacting in the Gulf of Mexico has shown the vulnerability of the present US oil storage facilities and refineries. The damage due to hurricanes Katrina and Rita in 2005 is yet to be known, but about 20% of the oil refinery capacity was affected and about 50% of the US production of oil was lost. Part of the losses corresponds to damage to aboveground storage tanks used to store oil along the coast of the Gulf of Mexico. Of course, this is not a new situation since buckling of tanks has been extensively reported in the Caribbean Islands and in the Southeastern coast of the US during the last 15 years. And this is not exclusive of the Atlantic shores, but also occurs in the Pacific and Indian Oceans as typhoons hit oil facilities.

Research in the buckling of steel storage tanks under extreme wind conditions is a rather recent topic. Studies in Europe have concentrated on lower wind speed conditions (Ressinger and Greiner

[†] Assistant Professor, E-mail: gportela@uprm.edu

[‡] Professor and Director, Corresponding Author, E-mail: lgodoy@uprm.edu.

1982) or have investigated geometries that are more representative of silos, with height to diameter ratios larger than one (Esslinger, *et al.* 1971). Storage tanks, on the other hand, are characterized by low height to diameter ratios, with values below 1. For such short tanks, the initial problem is the limited information about the distribution of pressures in the cylindrical part and in the roof of a tank. The current information arising from research in wind tunnels covers the pressures acting in isolated tanks (Sabransky and Melbourne 1987, Macdonald, *et al.* 1988, Portela and Godoy 2005a, 2005b).

But there are many situations in which tanks cannot be considered in isolation from their neighbors, and this is typical of tank farms in which the structures are spaced at extremely short distances because of lack of space in the oil facility. In a previous work (Portela and Godoy 2005c), the authors investigated pressures in tandem arrays by means of wind tunnel tests. Tandem arrays are present in some well designed tank farms with equal spacing between tanks. On the other hand, a common situation observed in oil refineries and industrial plants is a non-uniform array of tanks. In general, the configurations are not repeated from one refinery to another, and largely depend on the land available, the existence of previous tanks, and on the preferences of the owner and the designer.

This paper addresses the pressures in a group of tanks located in Yabucoa, Puerto Rico for which the dimensions of the tanks and their spacing are irregular, as shown in Fig. 1. Buckling damage was observed in one of the tanks (40 ft diameter and 45 ft height) after hurricane Georges in 1998. During this event the maximum wind gusts reported in the region were in the order of 130 mph. Small scale tests were carried out in a wind tunnel to obtain pressures, and such loads were next used to carry out a buckling analysis of the target tank in order to understand how the wind and structural configuration led to the observed failure.

2. Wind tunnel experiments to evaluate pressures in groups of tanks

Experiments were performed in the wind tunnel laboratory of the Civil Engineering and Surveying Department at the University of Puerto Rico in Mayagüez. The wind velocity profile was

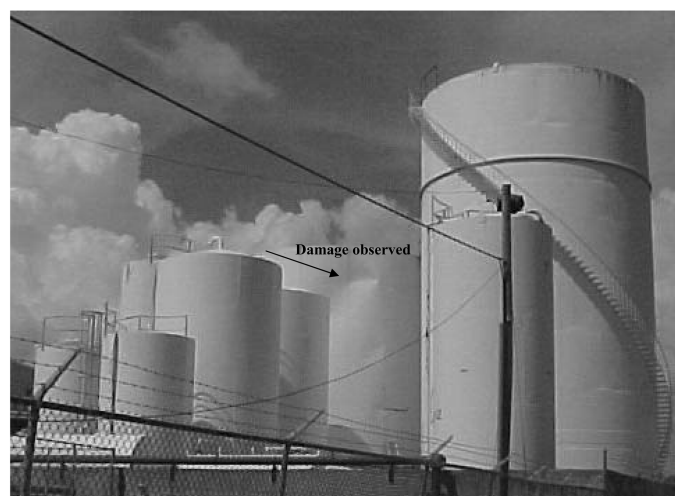


Fig. 1 Group of tanks located in Puerto Rico. The tank at the center buckled under hurricane winds.

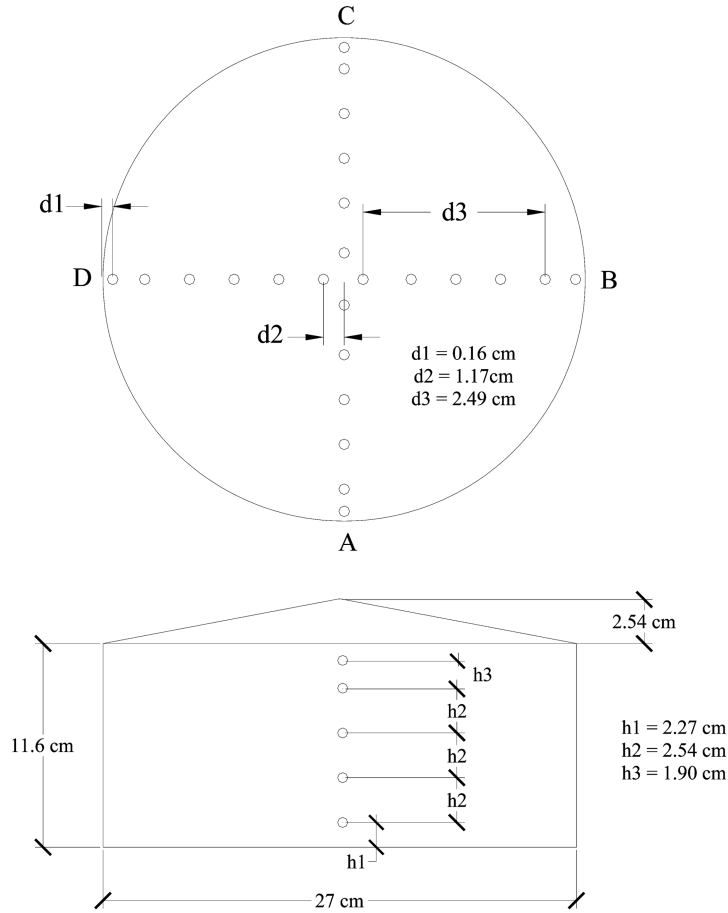


Fig. 2 Pressure taps on the roof and the wall of the experimental model

generated based on the following logarithmic equation:

$$V(z) = \frac{1}{\kappa} u_* \ln\left(\frac{z}{z_0}\right)$$

where V is the wind velocity at a specific elevation, z is the elevation from surface terrain, z_0 is known as the aerodynamic roughness length (based on a full-scale open terrain value of 0.02 m), κ is the von Karman constant (assumed as 0.4), and u_* is the friction velocity.

The roof was instrumented with twenty four pressure taps (six for each meridian at 90°), and the cylinder was instrumented with twenty pressure taps (five per quadrant), as shown in Fig. 2. The sample rate used for data acquisition consists of 800 samples per second and a sampling time of about 10 seconds was used. The values of four tunnel runs were averaged to obtain the pressure coefficients at the locations of the pressure taps. The target tank was rotated in order to obtain a complete sequence of measurements all around the tank. Figs. 3 and 4 depict two of the geometrical configurations considered by the authors in order to identify patterns of pressures produced in the target tank for which buckling occurred. The dimensions of the models tested in the wind tunnel facility are presented in Table 1, whereas photographs of the final models in the two configurations

Table 1 Dimensions of small scale models used in the wind tunnel experiments

| Tank | Configuration | Diameter [cm] | Height [cm] | H:D |
|------|---------------|---------------|-------------|--------|
| A | 1 | 26.92 | 11.57 | 0.43:1 |
| | 2 | 26.92 | 11.57 | 0.43:1 |
| B | 1 | 12.70 | 19.65 | 1.55:1 |
| | 2 | 9.50 | 10.79 | 1.14:1 |
| C | 1 | 5.70 | 7.60 | 1.33:1 |
| | 2 | - | - | - |
| D | 1 | 12.00 | 8.26 | 0.69:1 |
| | 2 | 12.00 | 8.26 | 0.69:1 |
| E | 1 | 12.00 | 8.26 | 0.69:1 |
| | 2 | 12.00 | 8.26 | 0.69:1 |
| F | 1 | 4.76 | 5.08 | 1.07:1 |
| | 2 | 4.76 | 5.08 | 1.07:1 |

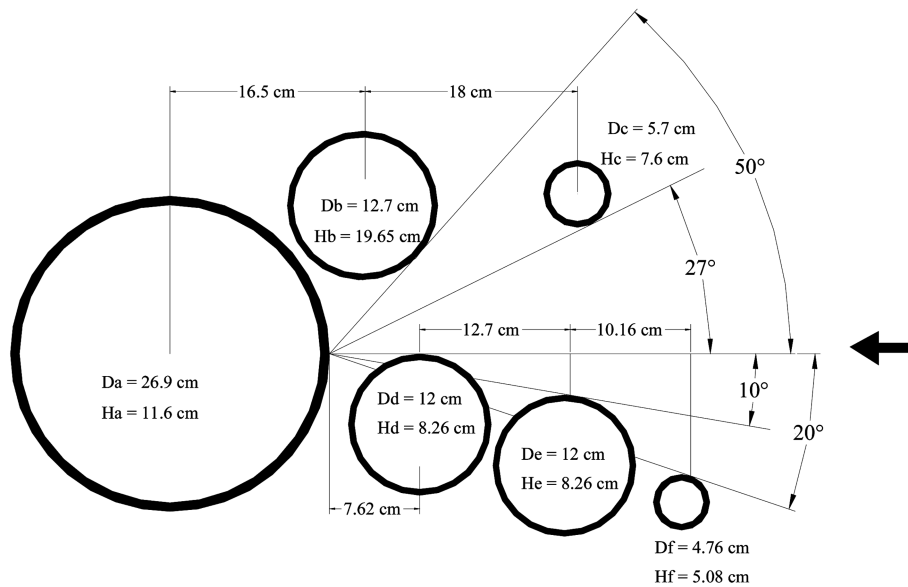


Fig. 3(a) First small scale configuration based on the group of tanks shown in Fig. 1

are shown in Figs. 3(b) and 4(b).

Two different wind directions in configurations T1 and T2 were considered. The second configuration had to be adjusted using smaller dimensions for the tank described as “B” in order to avoid corrections to account blocking effects. For this reason, the diameter of tank “B” in configurations 1 and 2 was changed from 12.7 cm to 9.50 cm and its height was changed from 19.65 cm to 10.79 cm.

In the first configuration, the scaled models “A”, “D”, “E”, and “F” were constructed using tubes

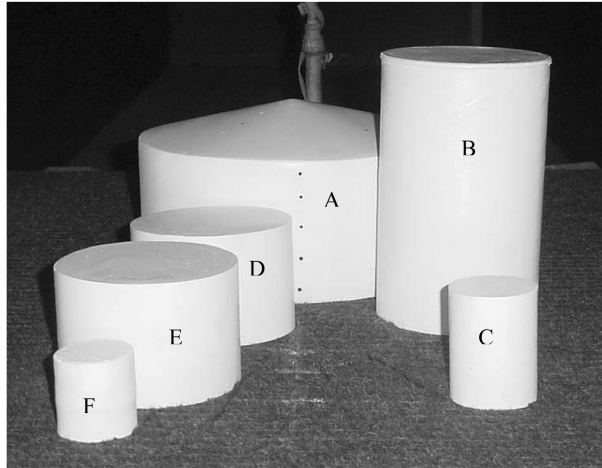


Fig. 3(b) Models representing the first configuration used in the wind tunnel experiments

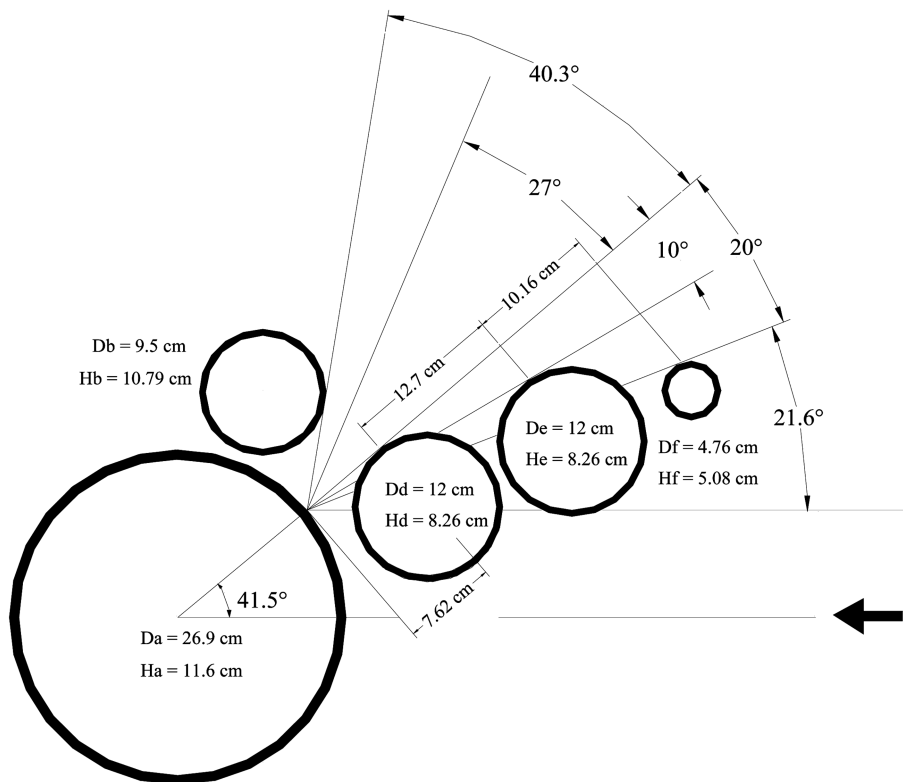


Fig. 4(a) Second small scale configuration based on the group of tanks shown in Fig. 1

of polyvinyl cement (PVC), while model “B” is an aluminum tube and model “C” was formed using a steel rod. Because of the low weight of model “F”, it was filled inside with lead so that it became stable under wind. In the second configuration, the models “A”, “D”, “E”, and “F” are the

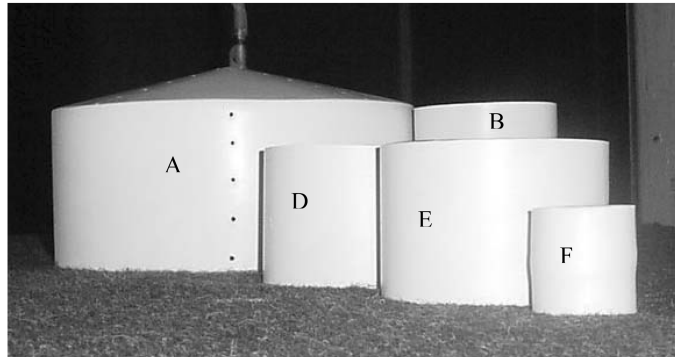


Fig. 4(b) Models representing the second configuration used in the wind tunnel experiments

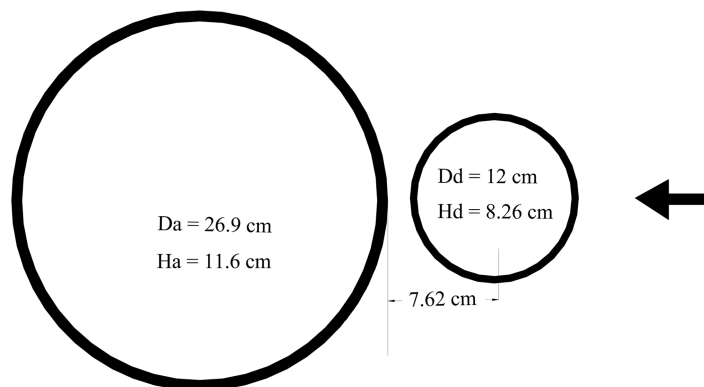


Fig. 5 Third small scale configuration based on a tandem array

same models used in the former configuration, but model “B” is a steel rod. As in the previous models investigated by the authors (Portela and Godoy 2005c), the roofs were constructed using a lightweight adhesive filler material and the surfaces were fixed to eliminate scratches, and were subsequently painted and polished.

A third configuration, shown in Fig. 5, was studied by just considering two tanks, i.e. those identified as “A” and “D” and used in the two previous arrays. This case is not a direct scenario of the group array observed in Fig. 1, but is a simplification with a tandem array. This case was studied because it had been previously observed that lower tanks shielding higher tanks produced a pressure increase due to the separation of wind flow at the wall-roof transition. This case differs from the previous tandem arrays because the tank exerting a shield (tank “D”) is considerably smaller in diameter and in height than the shielded tank (tank “A”), and because of the short distance separating them.

3. Wind tunnel results for the first configuration (T1)

Fig. 6 shows the pressure distribution measured from the first configuration (which is identified here as T1). Only one tank has been instrumented in the wind tunnel, and the results are presented

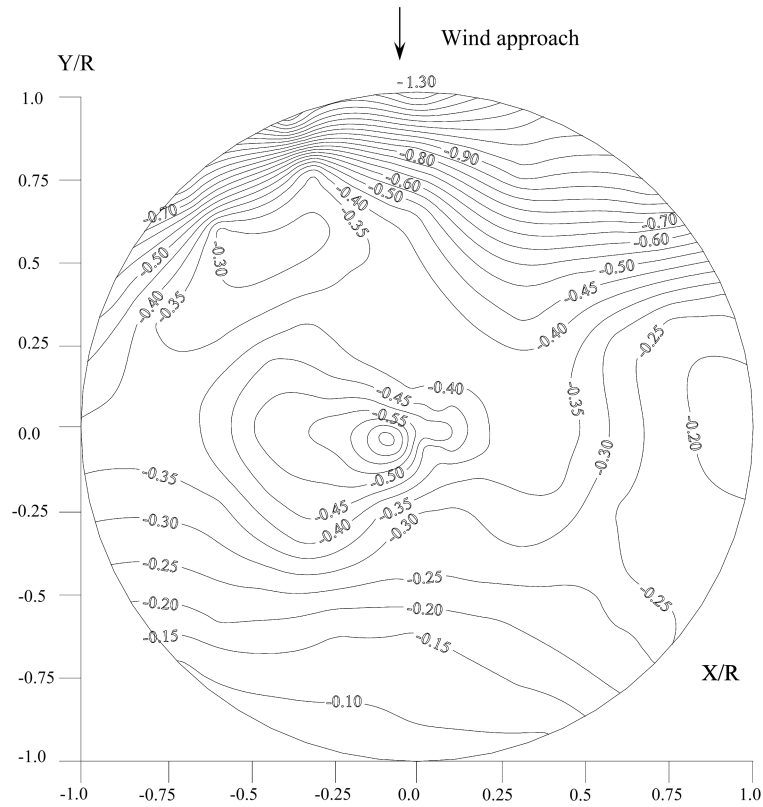


Fig. 6(a) Contours of the pressure coefficients on the roof using the first configuration

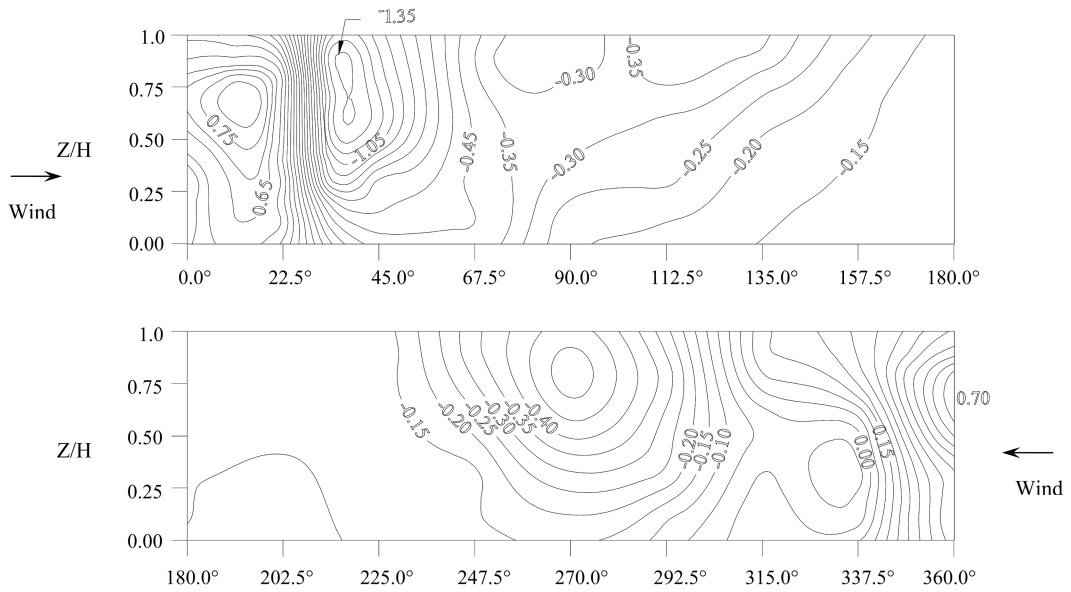


Fig. 6(b) Contours of pressure coefficients around the wall for the first configuration

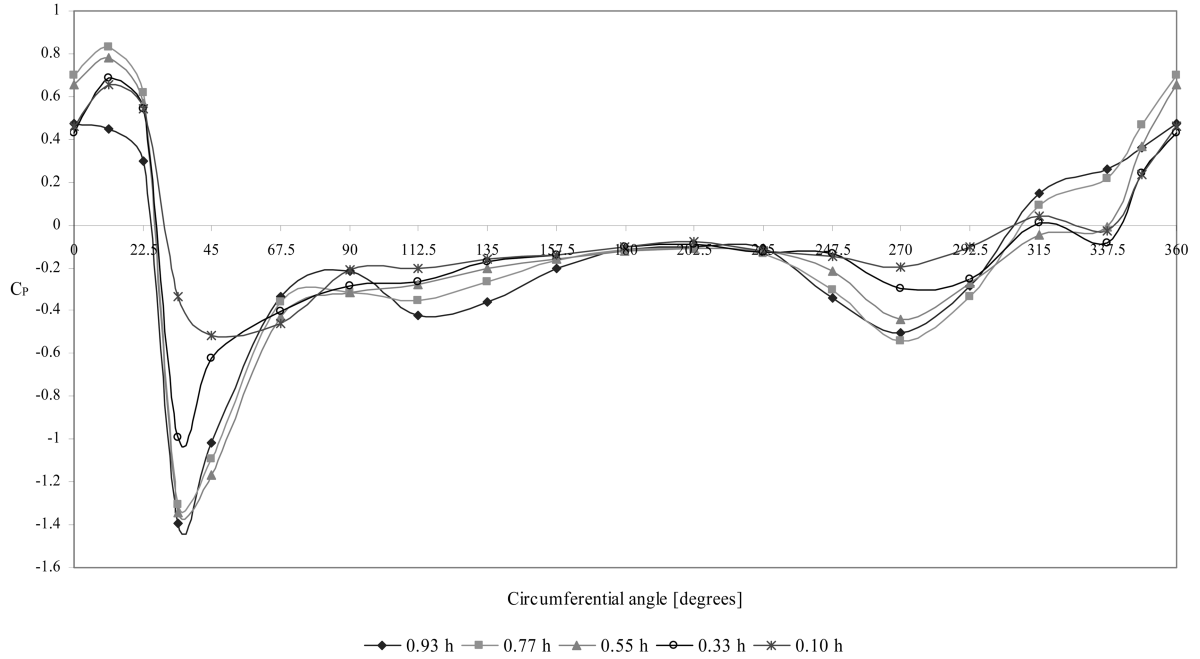


Fig. 6(c) Measured data around the wall of the first configuration

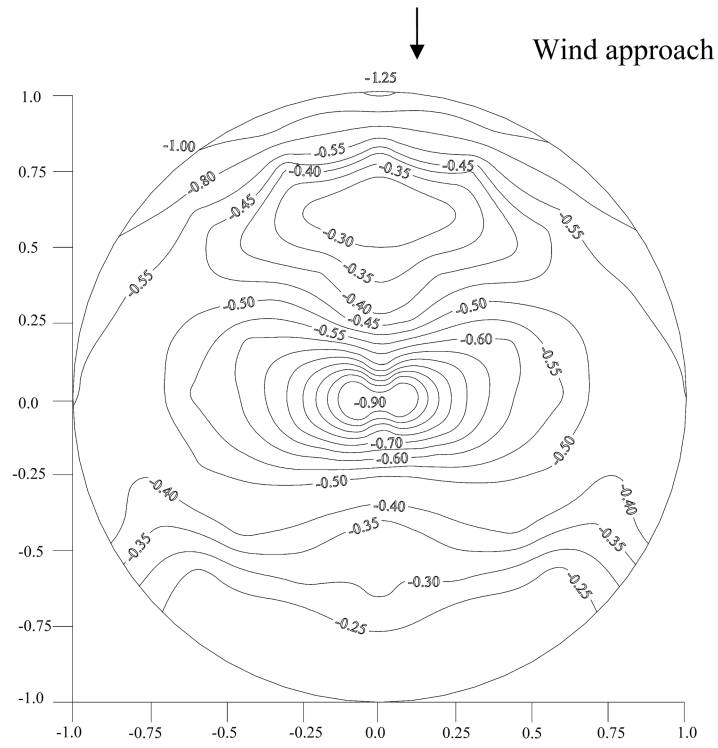
in non-dimensional form, using pressure coefficients C_p defined as

$$C_p = \frac{P_L}{P_d}$$

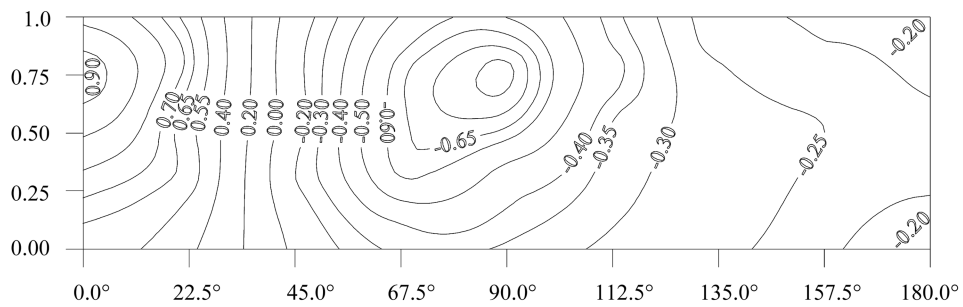
where P_L is the local dynamic pressure, and P_d is the dynamic pressure of reference at an equivalent height of 10 m.

Negative pressures (suctions) were obtained on the roof, with a maximum value measured at the wind entrance. The same tank was considered in isolation, as reported in Portela and Godoy (2005b). The pressures for the isolated case are shown in Fig. 7(a), and the results at the windward meridian of the roof are similar to those in Fig. 6 for configuration T1; however, significant differences were found in other sections of the roof. Moving forward from the windward meridian to the center of the roof, a different pressure distribution is observed as if the pressures in the isolated tank were rotated counterclockwise. This effect would be produced by the acceleration experimented by the flow between tanks “A” and “B” on the cylinder. The reason for an asymmetrical behavior may be due to differences in height between tanks “B” and “D”, as shown in Fig. 3(b). The maximum value observed at the highest region of the roof (in the isolated tank) was also shifted to a region close to 90 from the windward axis in T1. The maximum pressure recorded is $C_p = -0.74$, representing a 20% drop from the value in the isolated tank. In the leeward region of the roof, smaller pressure coefficients, in the order of $C_p = -0.10$, were observed, representing a 60% drop from the results in the isolated tank.

The results around the cylindrical part of the tank were measured by rotating the conical roof tank at intervals of 22.5° . Additional data was obtained at angles of 11.25° and 348.75° in order to have a better continuity of results in the region where maximum positive values were observed. Similarly,



(a) Roof



(b) Cylinder

Fig. 7 Wind pressure distributions obtained in the isolated tank

additional data was acquired at 33.75° in order to have a better estimate of the maximum negative pressures. The pattern of pressure distribution around the circumference of tank “A” was not symmetrical and was nonuniform. Both, maximum positive and negative (suction) pressures were found in the region delimited from 0° to 180° . Also, a reduction is observed in the region with positive pressure being reduced to 25° approximately, as observed in Fig. 6(b).

The height at which maximum positive pressures develop is in the range of $0.55 H$ to $0.75 H$, where H is the height of the cylinder. On the other hand, the lowest pressure coefficient obtained in the windward meridian corresponds to the higher ($0.90 H - 1.0 H$) and the lower ($0 - 0.30 H$) zones of the cylinder. In terms of the maximum negative pressure generated, these values were measured at heights from $0.55 H$ to $1.0 H$. Unlike to what happens in the isolated tank configuration, the maximum positive pressure coefficients in this case were shifted from an angle of 0° to an angle of 11.25° , corresponding to a value of $C_p = 0.83$. This behavior was also observed in the arrangement described by a tank with a conical roof shielded by a flat roof tank with similar dimensions and separated by a distance of $1/2 D$ (Portela and Godoy 2005c). However, for the same arrangement previously mentioned but separated by a distance of $1.0 D$, this effect was not observed. These results support the conclusion that tandem arrangements separated at close distances produce high changes in the pressure distribution at the windward region of the shielded tank.

Another aspect observed is that an increment in positive pressure does not occur at 348.75° (Fig. 6c). This behavior would happen because, as depicted in Fig. 3, tanks “D” and “E” block this region (348.75°), while at 11.25° there is no obstacle for the wind. Moreover, at 337.5° , negative pressure values are observed in the cylinder. Notice that the negative values in Fig. 6(c) develop at the lowest region of the cylinder. This behavior may be attributed to the wind flow interaction between tank “A” and tank “D”, as shown in Fig. 3(a). The maximum negative values were obtained at an approximate angle of 33.75° from the meridian of wind incidence developing a value of $C_p = -1.4$. Again, this region coincides with the wind flow interaction between two tanks (models “A” and “B”) and the observation of negative pressures along the complete height of the cylinder is due to the fact that both tanks have similar heights, unlike the case of models “A” and “D” with different heights. At an angle of 180° , the negative pressures were reduced to values lower than $C_p = -0.15$, representing a reduction in the order of 25% with respect to the isolated tank case.

4. Wind tunnel results for the second configuration (T2)

For this array, the models used as obstacle do not exceed the height of the instrumented model “A”. The negative pressure coefficients obtained on the roof of the second configuration (T2) are presented in Fig. 8(a). In this case the pressure distributions present a more symmetric behavior about the windward axis in comparison with the former configuration. The maximum suction was measured at the windward region, with a value of $C_p = -1.29$, being similar to the maximum value recorded in the first configuration and representing a difference of 4% with respect to the isolated case. On the other hand, the maximum values at the center of the roof showed values of $C_p = -0.89$, representing a difference of 20% with respect to the first configuration and of 2% with the isolated tank. The pressures in the leeward region of the roof were reduced, ranging between $C_p = -0.12$ and -0.20 , being higher than results observed in the first configuration ($C_p = -0.10$) but smaller than the values in the isolated case ($C_p = -0.25$).

The pressure distribution observed on the cylinder of the second configuration is shown in Fig. 8(b). Similar to the first configuration, an unsymmetrical pressure pattern is measured about the

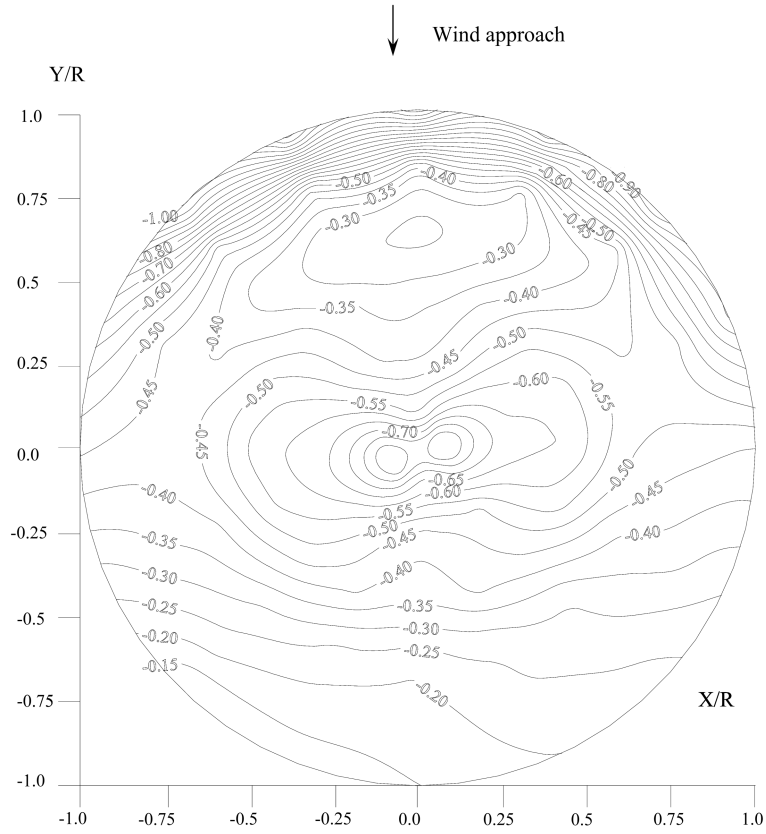


Fig. 8(a) Contours of pressure coefficients on the roof using the second configuration

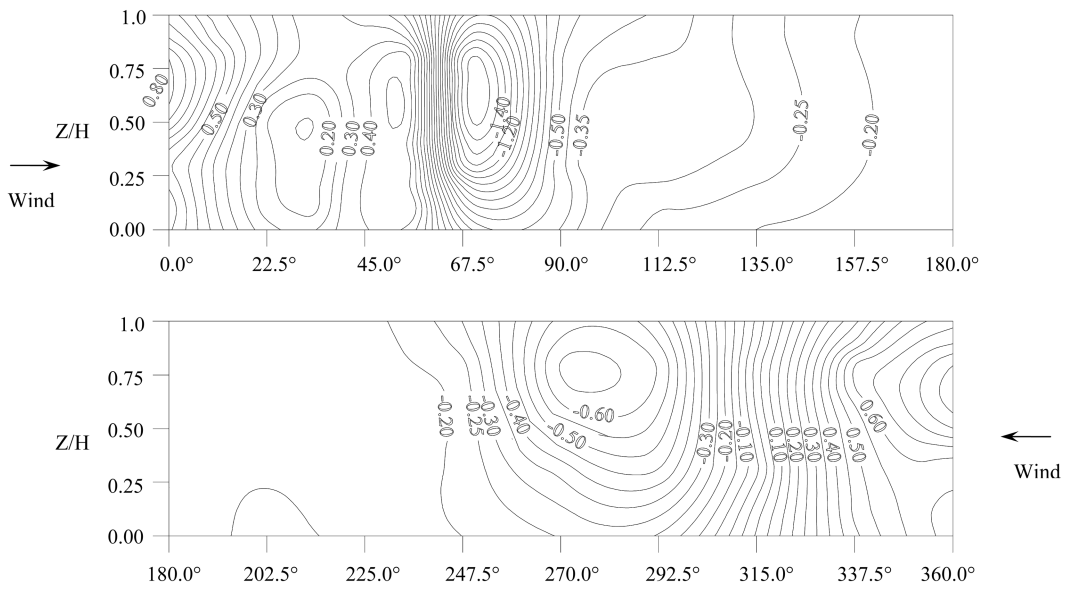


Fig. 8(b) Contours of pressure coefficients around the wall using the second configuration

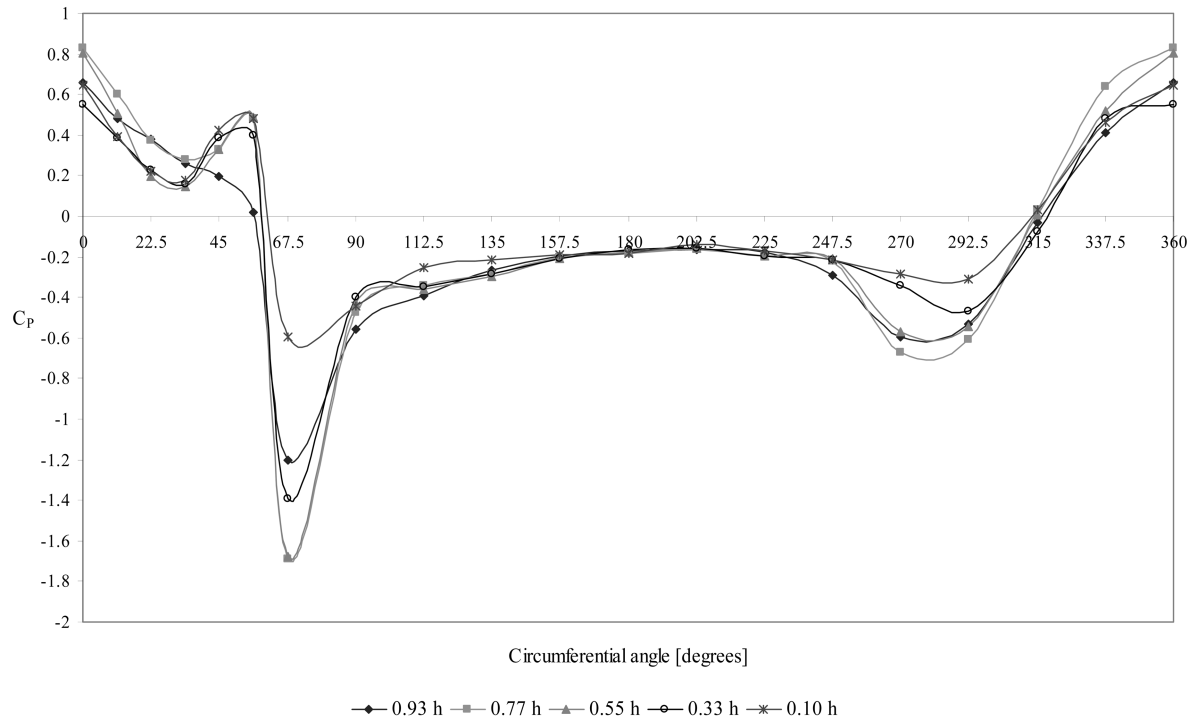


Fig. 8(c) Measured data around the wall of the second configuration

windward meridian. However, the region experimenting positive pressures extends to approximately 60° from the windward axis (Fig. 8c). In the other half (360° to 180°), the positive pressure spreads from 360° to 315° . This was the common region at which positive values were observed in the cases of isolated tanks (0° to 45° and 360° to 315° , approximately).

Moreover, the positive and negative pressure distributions observed from 360° to 180° are similar to those developed in the isolated case, but the absolute magnitudes are lower. This reduction would be due to the overall velocity reduction experimented by the wind interacting with the blocking tanks. In this region, both the maximum positive and negative values were observed between $0.6 H$ to $0.75 H$, approximately. On the other hand, the positive values have a tendency to reduce from 0° to 33.75° , followed by an increase observed from 33.75° to 56.25° , except for the higher region of the tank, which continues with a decreasing behavior (Fig. 8b). The heights where maximum pressures were observed in this region are in a range between $0.50 H$ to $0.80 H$. The maximum suction occurs between 67.5° and 90° and at heights from $0.55 H$ to $0.80 H$, with a maximum $C_p = -1.69$. This value represents an increase of 21% from the maximum negative pressure developed in the first configuration ($C_p = -1.4$). The lowest negative values were obtained close to the leeward region of the cylinder (202.5° , as shown in Fig. 8c) with values in the order of $C_p = -0.15$. These values are similar to the minimum suction observed in the first configuration (T1).

Fig. 9 shows the higher positive and negative pressure coefficients measured at different heights in the cylinder of the isolated tank and the group configurations MT1 and MT2. In the three cases, the highest positive C_p values were measured close to $0.75H$. The highest negative values in the isolated case and in configuration MT2 were also obtained close to $0.75H$. However, in configu-

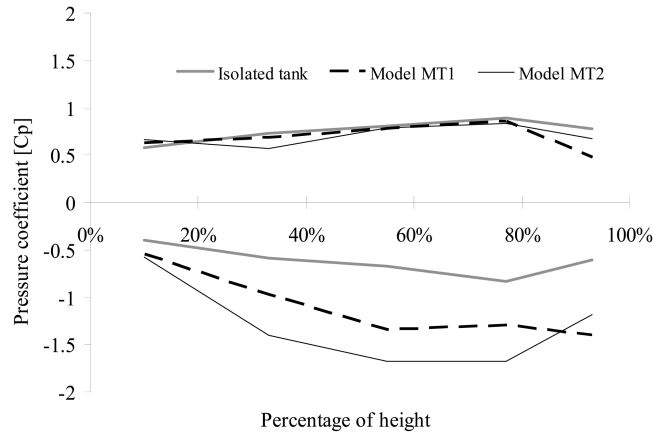


Fig. 9 Maximum pressure coefficients measured at different heights of the cylindrical models

ration MT1, the highest negative values were recorded at the top region of the wall (close to 90% of H). This value corresponds to an angle of 33.75° from the windward meridian.

5. Wind tunnel results for the third configuration (T3)

Similar to the previous two configurations, negative pressure coefficients were measured on the roof of the third configuration, as shown in Fig. 10(a). The pressure pattern is almost symmetrical with respect to the meridian of wind incidence. Maximum values were found at the entrance and in the central part of the roof, with values close to $C_p = -0.85$ for both regions. This represents a reduction on the windward area of the roof in the order of 35% with respect to the first (T1) and second (T2) configurations. However, comparing the values obtained at the central region of the roof, an increment of 15% occurred with respect to the first configuration (T1) and a reduction of 4% with respect to the second array (T2). Compared with the values found in the isolated tank with conical roof, these represent reductions in the order of 30% and 5% for the windward and center regions, respectively. The lowest values measured were located in the leeward region of the roof, with approximate values of $C_p = -0.12$. This value matches the range found in the two previous configurations (T1 and T2) at this region.

Contours with the pressure coefficients found on the cylindrical wall of the third configuration studied (T3) are presented in Fig. 10(b). Both hemispheres, the 0° – 180° (right hemisphere referenced from the windward meridian) and the 360° to 180° (left hemisphere) presented only small changes in the distributions. One aspect observed is that the region of positive pressures extends more in the right hemisphere (from 0° to 50°), and less (from 360° to 315°) in the left hemisphere (see Fig. 10c). The reason for this behavior would be due to variations in the location of the tank used as shield. The maximum positive value ($C_p = 0.99$) was on the meridian of incidence at the higher part of the cylinder. Maximum values at this region would be caused by the flow shedding from the smaller cylinder (“D”). On the other hand, the maximum negative values were observed at 75% to 100% the height of the cylinder. The maximum suction measured corresponds to a $C_p = -0.83$ located at 270° , being the same pressure observed in isolated tanks. As for the other cases, the lowest magnitudes of negative pressure were found at the leeward region of the cylinder with values close to $C_p = -0.15$.

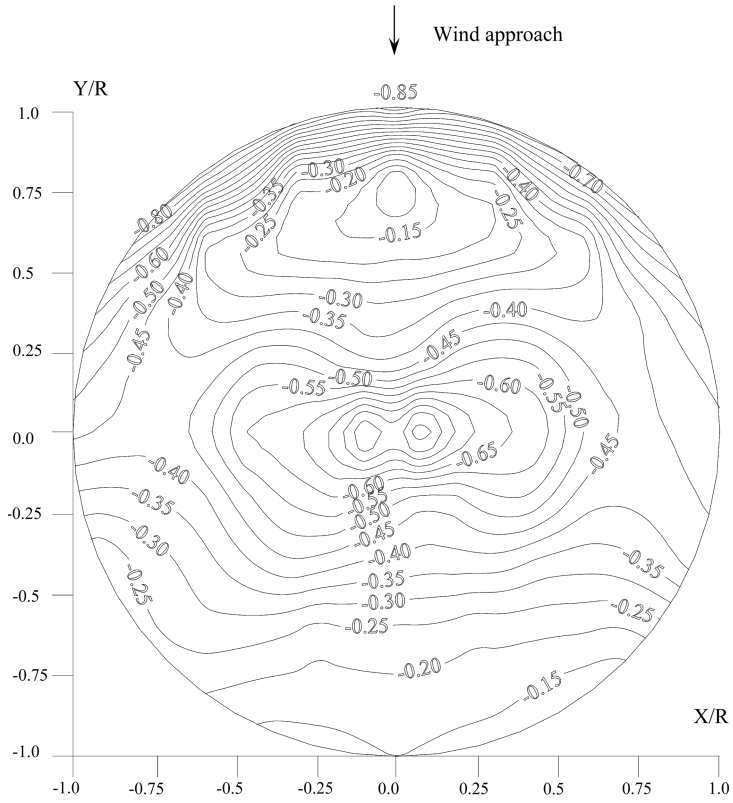


Fig. 10(a) Contours of pressure coefficients on the roof using the third configuration

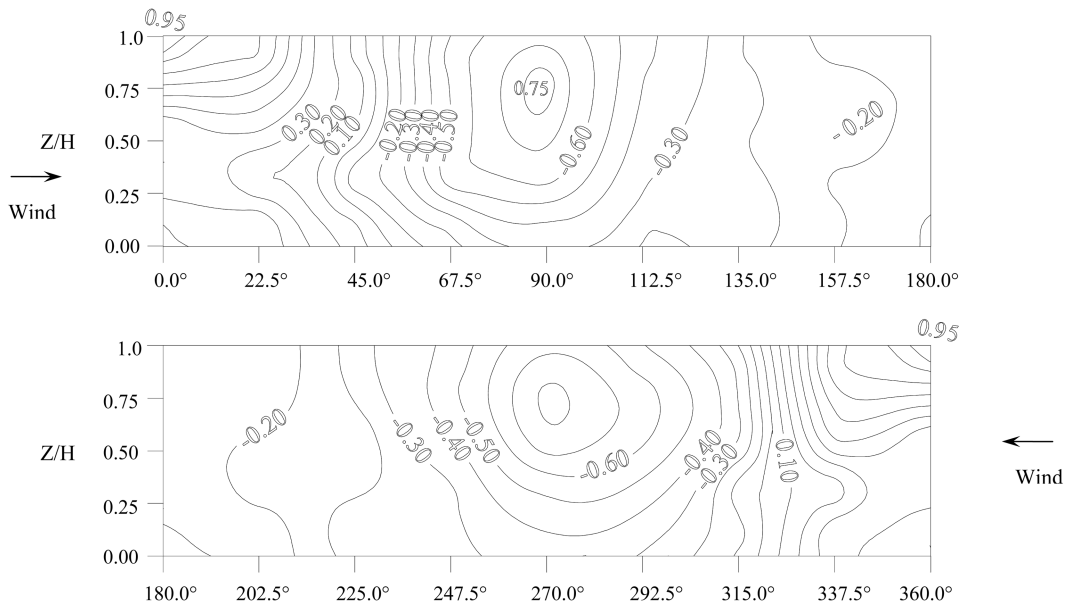


Fig. 10(b) Contours of pressure coefficients around the wall using the third configuration

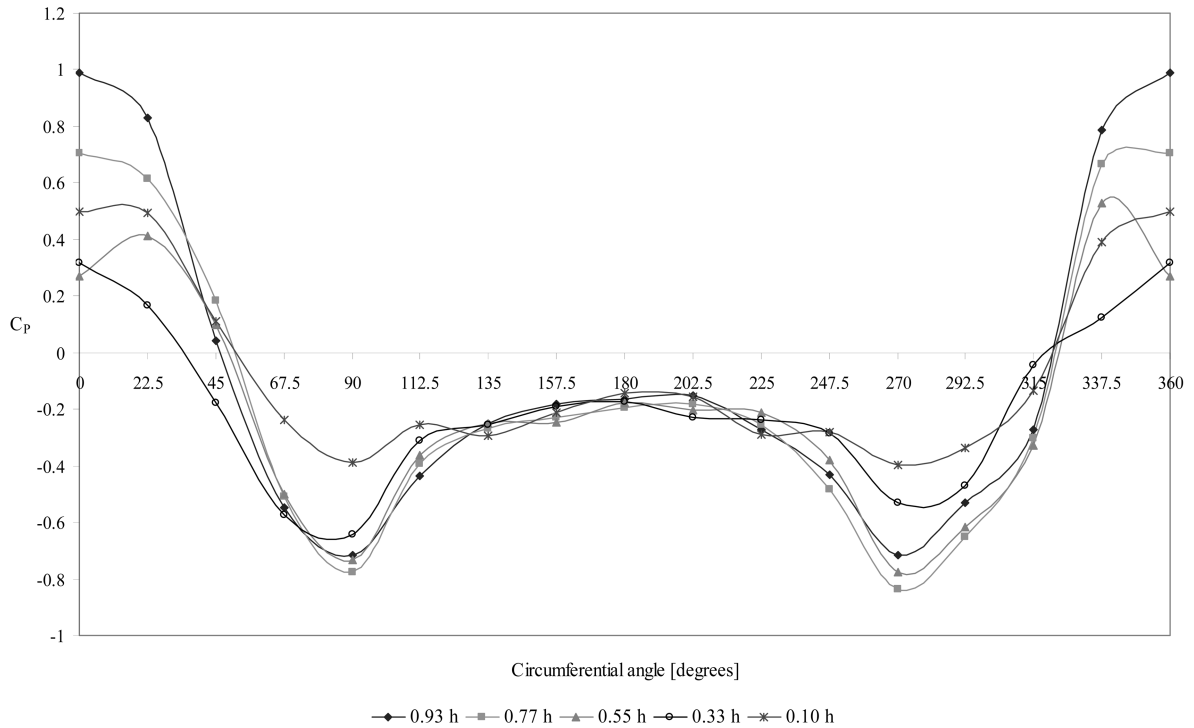


Fig. 10(c) Measured data around the wall of the third configuration

Table 2 Shell elements on the roof and the cylinder of computational models MT1, MT2 and MT3

| Computational model | Elements | |
|---------------------|----------|----------|
| | Roof | Cylinder |
| MT1 | 2,436 | 1,408 |
| MT2 | 2,260 | 1,408 |
| MT3 | 2,322 | 1,408 |

6. Computational buckling results

Computational models were generated using a general purpose finite element package (ABAQUS, 2002). The roof of the models was discretized with triangular shell elements using quadratic interpolation and the cylinder with rectangular shell elements. Table 2 presents the number of elements used for the roof and the cylinder of the modeled tanks. The number of elements used for the tanks exceed the minimum number of elements for the roof (1,916) and for the cylinder (1,408) established by means of a “ p ” and “ h ” type convergence analyses.

The wind pressure distributions T1, T2 and T3, obtained from wind tunnel experiments were applied to the finite element models MT1, MT2 and MT3, respectively. For each model, the buckling load and deformation was computed using both eigenvalue and geometric nonlinear analyses. The buckling loads were associated with the input wind loads by means of the load factor λ .

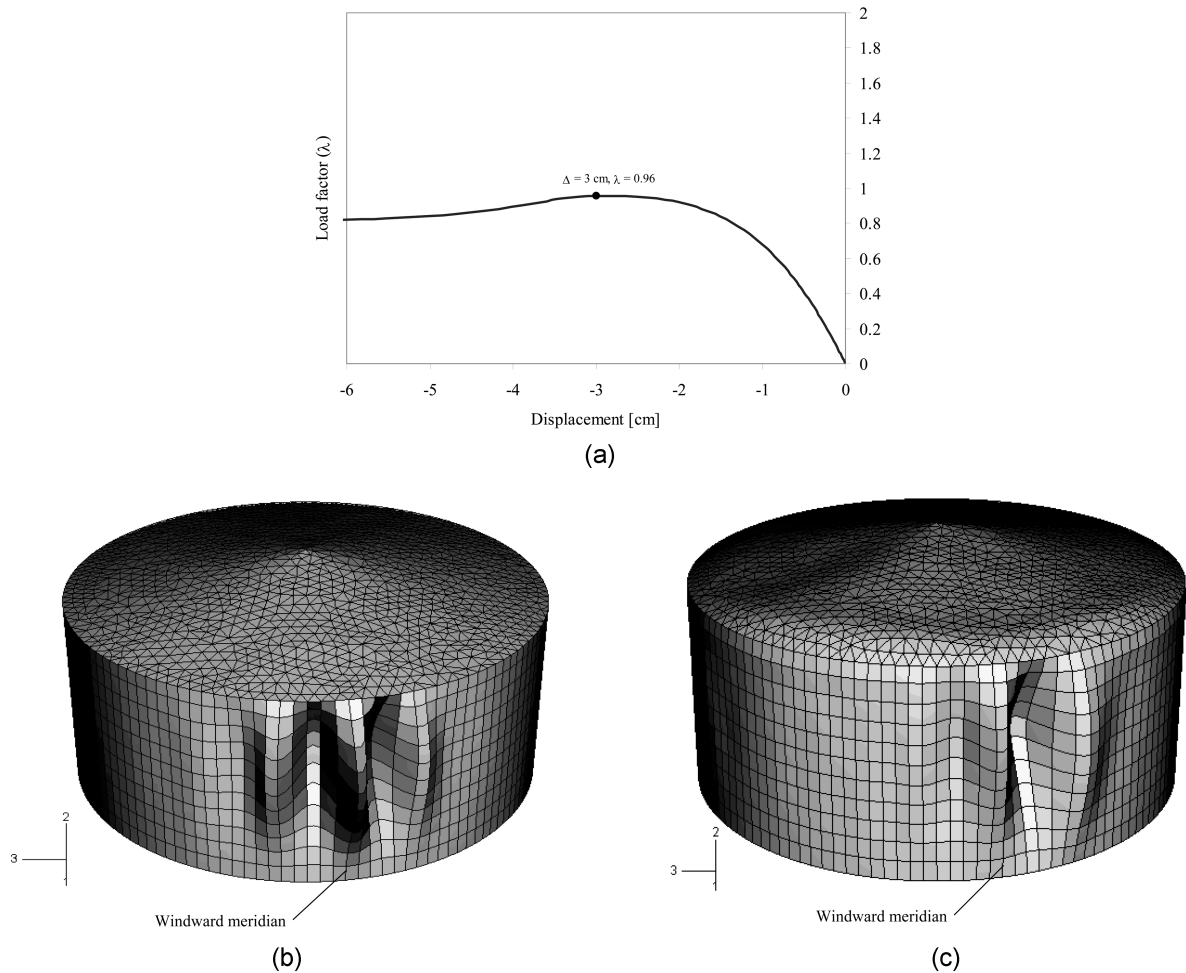


Fig. 11 Computational buckling results for model MT1. (a) Equilibrium path for a perfect configuration; (b) Eigenmode obtained from bifurcation analysis, $\lambda_c=1.22$; (c) Deformation from geometrically nonlinear analysis at the critical state, $\lambda_c=0.96$

The critical load is obtained by multiplying the critical load factor (λ^c) by the reference wind load assuming an unchanged wind profile during the load process. A value of $\lambda=1$ is associated to a reference wind speed of 145 mph.

The results for configuration MT1 are presented in Fig. 11. First, a bifurcation analysis (obtained from the solution of a classical eigenvalue problem with ABAQUS) was carried out in order to have an estimate of the range of values expected. Bifurcation solutions yield an upper bound to the expected wind buckling loads, and in this case a critical load $\lambda=1.22$ was computed. The associated eigenmode is shown in Fig. 11(b).

Next, a geometrically nonlinear analysis was performed for the perfect geometry of the shell using the pressure distributions obtained in the wind tunnel tests for T1, and the results are presented in Fig. 11(a) in the form of a load-deflection equilibrium curve. The path reaches a maximum load at $\lambda=0.96$ (that is, a reduction of 21.6% with respect to the bifurcation analysis). The lowest load

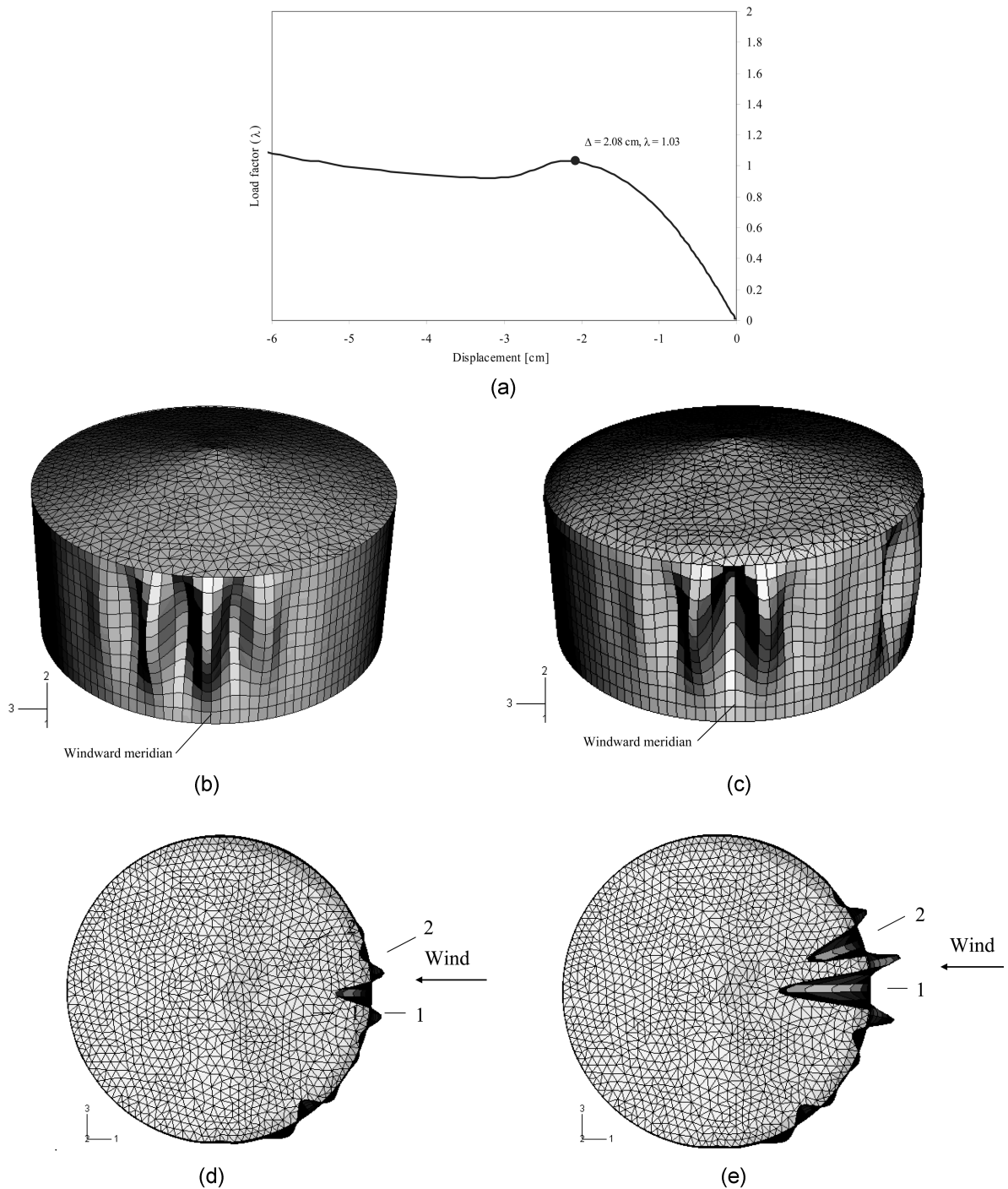


Fig. 12 Computational buckling results for model MT2. (a) Equilibrium path for a perfect configuration; (b) Eigenmode obtained from bifurcation analysis, $\lambda_c=1.19$; (c) Deformation from geometrically nonlinear analysis at the critical state, $\lambda_c=1.03$; (d) Deformations at the postbuckling unstable path for $\Delta=2.4$ cm; (e) Deformations at the postbuckling stable path for $\Delta=5.5$ cm

factor obtained from all nonlinear analyses was the one of model MT1.

The deflected shape at the maximum load is shown in Fig. 11(c). Large displacements were found in the windward region of the tank at the critical point. The global x , y , z coordinates of the node where maximum displacements were obtained are (15.24, 0, 8.34) m, with the origin located at the intersection between the axis of rotation of the shell and the plane at the base. The maximum displacement obtained in the critical node corresponds to a value of $\Delta = 2.91$ cm.

Differences between both bifurcation and nonlinear analyses for model MT1 were also observed in the buckling deformations, for example, the circumferential waves in the cylinder were reduced from three to two, as shown in Fig. 11(c). The differences between the simplified bifurcation analysis and more refined nonlinear analysis in terms of both critical loads and associated buckling modes, provide an indication that the bifurcation approach is not appropriate for this class of problem.

Results for the second configuration of tanks, i.e., model MT2, are shown in Fig. 12. The bifurcation load from an eigenvalue analysis was $\lambda = 1.19$, with the shape (given by the eigenvector) plotted in Fig. 12(b). In the nonlinear investigation of this tank, an initial unstable post-buckling behavior was observed, followed by a stable path, as shown in Fig. 12(a). As expected, the geometrically nonlinear analysis provided a smaller critical value, with $\lambda = 1.03$, whereas the displacement at the critical load was 2.08 cm. Considerable deformations occurred at an angle of approximately 65° from the windward meridian (Fig. 12c), which were not present in the eigenvector (Fig. 12b). It seems that these deformations are associated with the experimental positive pressure coefficients developed also at 65° from windward, as shown in Fig. 8(c).

The deformed shape of the tank was studied in both the unstable and stable paths in order to understand the nonlinear behavior of the structure. From Fig. 12(c), it seems that the most affected zone of the tank during the fundamental and initial post-critical paths was the region designated as "1". But, at considerable large displacements (Fig. 12d) more regions (i.e. region "2") began to deform.

The results for the third configuration, with pressures obtained from model MT3, are shown in Fig. 13. For the third case, a higher eigenvalue $\lambda = 1.47$ was obtained, whereas $\lambda = 1.38$ was computed from the nonlinear analysis (Fig. 13a), representing a 6.2% reduction. The mode shapes and deformations are shown in Figs. 13(b) and 13(c), respectively. Again, changes in the buckling modes were detected depending on the type of analysis.

7. Imperfection-sensitivity

The computations described in the previous section were made using the as-designed, or perfect geometry of the shell. Thanks to the pioneering work of Koiter (1945), it is now clear that shell structures are sensitive to the presence of unavoidable imperfections in the geometry. Thus, additional studies were carried out to investigate the influence of imperfections in the geometry of model MT1, which was the model for which the lowest critical load was computed in the previous section.

The shape of the imperfections is defined using the same geometry of the modal displacements resulting from the eigenvalue analysis, and the initial geometry of the tank was thus modified with imperfections of the same order as the thickness of the cylinder. Negative imperfections were oriented with outward maximum displacements and orthogonal to the surface of the cylinder, based on the first buckling mode shape.

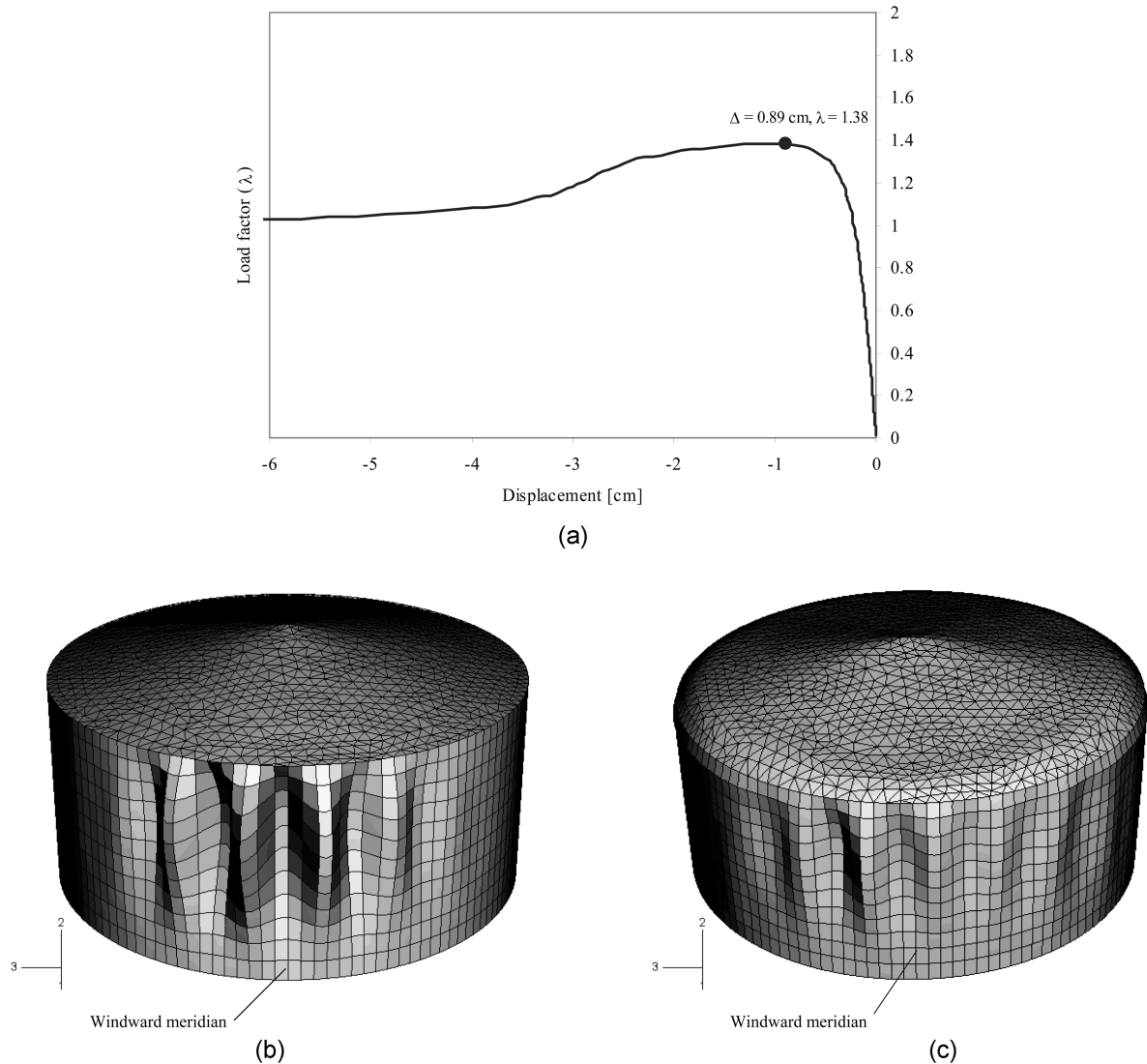


Fig. 13 Computational buckling results for model MT3. (a) Equilibrium path for a perfect configuration; (b) Eigenmode obtained from bifurcation analysis, $\lambda_c=1.47$; (c) Deformation from geometrically nonlinear analysis at the critical state, $\lambda_c=1.38$

From Fig. 11(a), the fundamental equilibrium path of the tank for a perfect geometry reaches a maximum and is followed by an unstable state. For small imperfections (with amplitude $\zeta \leq 0.5t$) the nonlinear path shown in Fig. 14(a) does not change dramatically the load-displacement response of the tank. But for larger imperfections, the equilibrium path displays large displacements and the point of maximum load vanished, with the consequence that the buckling problem is transformed into a large deflection problem.

Next, consider the mode shapes. For an imperfection amplitude of $\zeta = \pm 0.50t$, the deformed shapes computed at the first critical point of the equilibrium path were practically the same of those

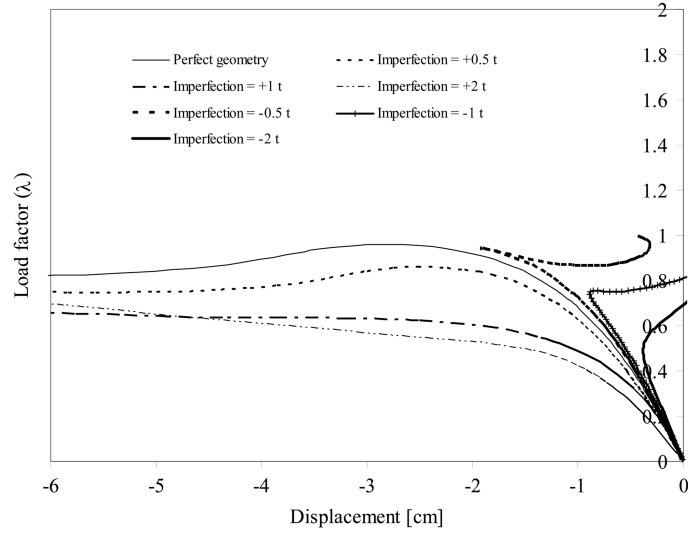


Fig. 14 Influence of geometric imperfections on the equilibrium paths of model MT1

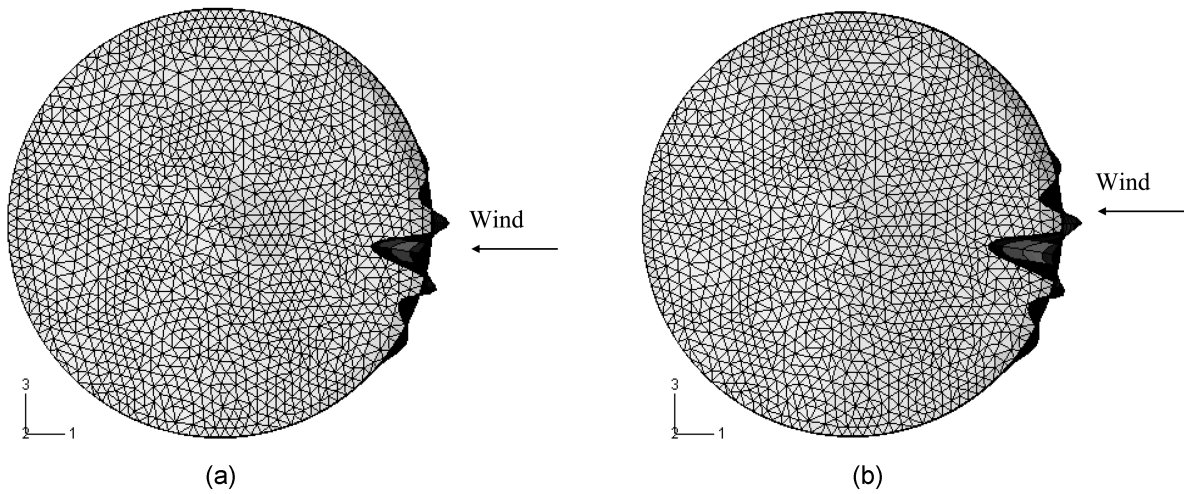


Fig. 15 Deformations at the critical load of model MT1 for: (a) $\zeta = -1.0t$ and (b) $\zeta = -2.0t$

obtained in the perfect geometry (Fig. 11c). However, large negative imperfections with values of $\zeta \geq -0.5t$ increase the stiffness of the tank and change its deformed shape, as seen in Figs. 15(a) and 15(b) for $\zeta = -1.0t$ and $-2.0t$.

The plot of imperfection-sensitivity for the isolated model and the first group configuration (MT1) is shown in Fig. 16. The curve of sensitivity of model MT1 shows reductions in the maximum loads due to imperfections of the order of 25%. This may be identified as a case of moderate imperfection-sensitivity, as most shells under lateral loads. From the figure, it seems that the isolated case is more sensitive to small and moderate imperfections than the group configuration MT1. Notice that most tanks have imperfections in the geometry due to construction defects (usually

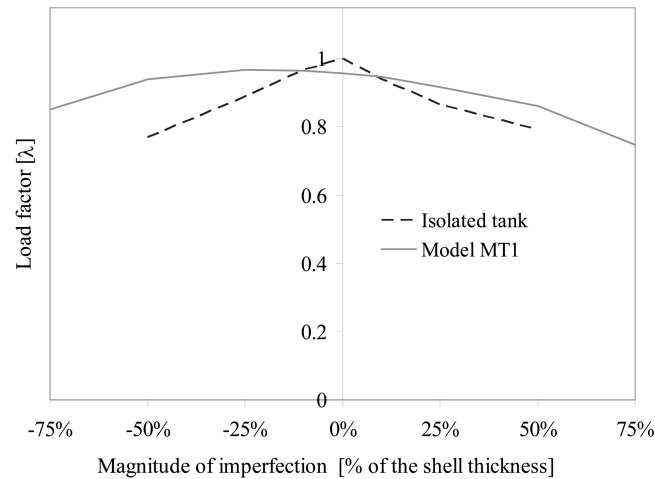


Fig. 16 Imperfection-sensitivity of the isolated tank and model MT1

small imperfections), deflections due to previous natural events (usually moderate to large imperfections) or due to problems caused during the operation of the facility, such as when the tank is suddenly emptied (usually large imperfections).

8. Conclusions

This paper employed a sequential experimental/computational methodology to investigate wind buckling in a tank that is part of a complex configuration. The group of tanks is considered in the experiments, in which three wind-tunnel configurations of rigid reduced-scale models were tested to obtain pressure coefficients in the target tank. The pressures were next used as loads in the computational buckling analysis of the deformable tanks. The main conclusions of the research may be stated as follows:

- The present experimental/computational approach seems to be capable of reproducing the real events in a full scale group of tanks under hurricane winds.
- For one of the grouped arrays of tanks (MT1), the critical pressure computed is slightly lower (by 4%) than in the isolated tank; however, the imperfection-sensitivity in the group of tanks is less pronounced than in the single tank.
- Results from the nonlinear analysis revealed unstable post-critical paths in all cases, except in model MT2, for which an initial unstable post-critical path was followed by a secondary stable path.
- The eigenvectors in the bifurcation analysis and the deformed shape (computed using a nonlinear analysis) of the tanks with perfect geometry had similar shapes. Thus it seems that a good choice of the imperfection shape (that would produce a more severe effect in reducing the maximum attainable load) is the eigenvalue itself.
- From the imperfection sensitivity analysis, it seems that the buckling capacity of the target tank (surrounded by others, as shown in Fig. 1), is reduced in the order of 25%. This value represents a reference wind velocity in the order of 56 m/s (125 mph) and is below the expected hurricane wind speed in the Caribbean region and the South Eastern US coast (ASCE 2002). This wind

velocity value is clearly below the wind speeds that may have occurred in this area of Puerto Rico during Hurricane Georges. The present study helps to explain that the buckling damage observed in the target tank occurred even if the tank had no corrosion or extensive previous damage due to other sources. As a lower bound to grouped tanks accounting for imperfections, the results show that an isolated tank yields critical wind speeds that are lower than those computed in more complex group arrays.

- The present results may serve as an illustration of what level of changes is expected between isolated tanks and groups of tanks. However, the present study is restricted to just a few configurations found in practice, and larger differences may be found in other configurations.

Acknowledgements

This research was supported by a grant from National Science Foundation: “SGER: Identification of structural damage in tanks and industrial facilities due to hurricane Katrina”, Award number 0553986, 2005-2006.

References

- ASCE 7 Standard (2002), *Minimum Design Loads for Buildings and Other Structures*. American Society of Civil Engineers, Virginia, USA.
- ABAQUS (2002), User manual-version 5.6. Pawtucket, RI, USA. Hibbit, Karlsson & Sorensen.
- Esslinger, M., Ahmed, S., and Schroeder, H. (1971), “Stationary wind loads of open topped and roof-topped cylindrical silos”, (in German). *Der Stahlbau*, 1-8.
- Koiter, W. T. (1945), “On the stability of elastic equilibrium”, Doctoral Dissertation, Delft (translated at NASA, Tech. Trans. F10, 833, 1967).
- Macdonald, P. A., Kwok, K. C. S., and Holmes, J. H. (1988), “Wind loads on isolated circular storage bins, silos and tanks: Point pressure measurements”, *Research Report No. R529, School of Civil and Mining Engineering*, University of Sydney, Sydney, Australia.
- Portela, G. and Godoy, L. A. (2005a), “Wind pressures and buckling of cylindrical steel tanks: Tanks with dome roofs”, *J. Constr. Steel Res.*, **61**, 786-807.
- Portela, G. and Godoy, L. A. (2005b), “Wind pressures and buckling of cylindrical steel tanks: Tanks with conical roofs”, *J. Constr. Steel Res.*, **61**, 808-824.
- Portela, G. and Godoy, L. A. (2005c), “Shielding effects and buckling of steel tanks in tandem arrays under wind pressures”, *Wind and Struct.*, **8**(5), 325-342.
- Resinger, F. and Greiner, R. (1982), “Buckling of wind-loaded cylindrical shells-application to unstiffened and ring-stiffened steel tanks”, *Buckling of Shells*, Ramn E. (ed.), Springer, Berlin, pp. 217-281.
- Sabransky, I. J. and Melbourne, W. H. (1987), “Design pressure distribution on circular silos with conical roofs”, *J. Wind Eng. Ind. Aerodyn.*, **26**, 65-84.